Texture Features for Classification of Ultrasonic Liver Images

Chung-Ming Wu, Yung-Chang Chen, *Senior Member, IEEE,* and Kai-Sheng Hsieh

Abstract—**In this paper, the classification of ultrasonic liver images is studied by making use of some powerful texture features, including the spatial gray-level dependence matrices, the Fourier power spectrum, the gray-level difference statistics, and the Laws' texture energy measures. Features of these types are used to classify three sets of ultrasonic liver images—normal liver, hepatoma, and cirrhosis (30 samples each). The Bayes classifier and the Hotelling trace criterion are employed to evaluate the performance of these features.**

From the viewpoint of speed and accuracy of classification, we have found that these features do not perform well enough, either consuming much time or yielding low classification rate. Hence, a new texture feature set (called multiresolution fractal features) based upon the concepts of multiple resolution imagery and fractional Brownian motion model is proposed to detect diffuse liver diseases fastly and accurately. In our approach, fractal dimensions estimated at various resolutions of the image are gathered to form the feature vector. Texture information contained in the proposed feature vector will be discussed. A real time implementation of our algorithm is performed on a SUN 4/330 workstation and produces about 90% correct classification for the three sets of ultrasonic liver images. This suggests that the multiresolution fractal feature set is an excellent tool in analyzing ultrasonic liver images.

I. Introduction

ULTRASONIC echoes from soft tissues, when displayed as a *B*-scan image, form a texture pattern that is characteristic of both the imaging system and the tissue being imaged. This image texture results from interactions between the coherent ultrasonic pulses transmitted into the body and the structure of the tissues. The correspondence between image texture and tissue's microstructure greatly depends on the size and spatial distribution of the tissue scatterers relative to the wavelength of the incident pulse. Ultrasonic measurements that describe the structure of soft tissues are potentially very useful tissue signature since one feature of diffuse and focal disease processes of liver is disruption of the normal tissue architecture [1].

Currently, most useful tissue differentiation techniques are based on the analysis of a *B*-scan image of the liver [1]–[7]. The radio-frequency (RF) signal produced by the transducer when it transforms the ultrasonic echoes into an electrical waveform requires only minimal processing, such as envelope detection, in order to produce an image. More extensive processing and filtering are used to further enhance image quality. This process of manipulating the RF signal results in a loss of phase information and, consequently, a loss of much of the information regarding tissue signature. Thus, some researchers [8] characterize liver disease using the raw RF signal. Although the use of raw RF data is attractive and has many advantages, it also has major drawbacks. At first, RF data must be sampled at a very rapid rate (usually in excess of 20 MHz). The amount of data stored and processed when using RF signals is thus much larger than that required when using image data. Furthermore, nonstandard equipment configurations may be needed. Hence, if we ignore the distortion caused by a *B*-scanned video image, the gray-level distribution of a *B*-scan image can be used to characterize liver tissues.

An ultrasound *B*-scan image is the result of a rather complicated set of physical phenomena, namely, the insonification and the resulting absorption, reflection, and coherent scattering from a tissue medium of pulsed ultrasonic pressure waves at radio frequency, and the electronic detection of the backscattered or echoed pulses for display as an image. The resulting pictures have the various granular structures described, as above, by "texture." Consequently, the analysis of ultrasonic images is analogous to the problem of texture classification. In the past few years, many statistical features which describe the physical properties of the tissue have been published to distinguish between normal and abnormal ultrasonic liver images [1]–[7]. Based upon these features, Insana and Garra *et al.* [4]–[6] use areas under the receiver operating characteristic (ROC) curve to evaluate the diagnostic performance of the methods and not accuracy. The classification error may be due to the fact that inadequate information was captured by the features. Hence, in this paper, the use of more powerful texture features for the detection of diffuse diseases using acoustic data is studied.

A number of approaches to the texture classification problem have been developed over the years. The most commonly used texture features that have been applied successfully to real-world textures are the spatial gray-level dependence matrices (SGLDM) [9], the Fourier power spectrum (FPS) [10], the gray-level difference statistics (GLD) [11], and the Laws' texture energy measures (TEM) [12]. The definitions of these features are summarized in Section II. In this paper, feature sets of these types are used to classify three sets of sampled ultrasonic liver images—normal liver, hepatoma (hepatocellular carcinoma), and cirrhosis.

Manuscript received May 29, 1991; revised December 18, 1991. This work was supported in part by the National Science Council of the Republic of China under Grant NSC 80-0404-E007-05.

C.-M. Wu and Y.-C. Chen are with the Department of Electrical Engineering, National Tsing Hua University, Hsinchu, Taiwan 30043, Republic of China.

K.-S. Hsieh is with Veterans General Hospital, Taipei, Taiwan 11221, Republic of China.

IEEE Log Number 9107155.

To evaluate the performance of these conventional features, the Bayesian classifier [13], [14] and the Hotelling trace criterion [15] are applied to determine the feasibility of classifying tissue types as well as determining some properties of various feature spaces. From experimental results it can be found that these conventional features perform no better than the physical properties based features. Hence, we have concluded that these features do not catch the important information of ultrasonic liver images—granularity. Consequently, a more suitable feature set to describe the property of granularity (or similar property) is needed for the classification of liver tissues.

The fractal concept developed by Mandelbrot [16] provides an excellent representation of the ruggedness of natural surfaces. It has been successfully applied to geographical simulation [17], texture analysis [18], [19], and X-ray medical images [20]. One of the most important fractal models to describe natural fractal phenomena is the fractional Brownian motion (fBm) model which is proposed by Mandelbrot [16]. It regards naturally occurring rough surfaces as the end result of random walks. Such random walks are basic physical processes in our universe. An intensity surface of an ultrasonic liver image can also be viewed as the end result of a random walks, so the fBm model can be suitable for the analysis of ultrasonic liver images. Two of the most important parameters to characterize a fractal surface are the fractal dimension and lacunarity, which measure the roughness and granularity of the surface. Hence, the fractal dimension and lacunarity which measure the roughness and the granular structure of an image are the most important features in the classification of ultrasonic liver images. Recently, Chen [21] defined a feature vector based on normalized fractional Brownian motion (NFBM) to represent the statistical characteristics of the medical image surfaces. He applied the feature vector to five different ultrasonic images and concluded that the classification of normal and abnormal ultrasonic liver images could be obtained from the differences between their NFBM feature vectors. The drawback of the NFBM feature vector is two fold. 1) It tends to be time consuming. About M^4 operations are needed to estimate the NFBM feature vector of block size $M \times M$. For a 27×27 image, Chen said that it took about $1/2$ h to compute the fractal dimension by using a standard personal computer (PC/AT). 2) The NFBM approach causes some information distortion. For example, for a given scale Δr, say $\Delta r = 4$, the expected gray-level difference of pixel pairs separated by distance Δr should be the pairs $\{(x_1, y_1), (x_2, y_2) : (x_2 - x_1)^2 + (y_2 - y_1)^2 = 4^2\}$. The pixel pairs measured by NFBM are $\{(x_1, y_1), (x_2, y_2) : 16 \leq (x_2 - x_1)^2 + (y_2 - y_1)^2 < 25\}$. That is to say, the NFBM feature represents the summation of the statistical information at scales 4, 4.123, 4.242, and 4.472, instead of the intrinsic statistical information at the integer scale $\Delta r = 4$. To overcome these two disadvantages, the estimation method proposed by Pentland [19] is modified to extract the fractal dimensions of the image.

In general, a single fractal dimension is unable to discriminate most of the real-world textures. Hence, the term "lacunarity" is introduced to describe the characteristic of fractals of the same dimension with different appearances or textures [16], [22], [23]. Given a fractal set A, let $P(m)$ be the probability that there are m points within a box of size L centered about an arbitrary point of A. We have $\sum_{m=1}^{N} P(m) = 1$ where N is the number of possible points within the box. Voss [22] defined the lacunarity as

$$\Lambda = \left(M_2 - M^2\right)/M^2 \tag{1}$$

where

$$M = \sum_{m=1}^{N} mP(m)$$

$$M_2 = \sum_{m=1}^{N} m^2 P(m).$$

The second-order statistic, lacunarity, is small when the texture is dense and large when the texture is coarse. The lacunarity measurement can not be estimated directly from a modified procedure. Thus, a further technique is needed not only to solve this problem but also to preserve the computational effort. Recently, the technique of multiple resolution feature extraction has been pointed out to be an efficient way to describe textures. Let us suppose that there is a sequence of increasing resolutions (α_j), j is an integer and α is a resolution step. If the camera gets α times closer to the scene, each objects of the scene is projected on an area α^2 times bigger in the focal plane of the camera. Based on this concept, Burt [24] and Crowley [25] introduced pyramidal implementation for computing the signal details at different resolutions. Burt has chosen a step $\alpha = 2$. The details at each resolution 2^j are calculated by filtering the original image with the difference of two low-pass filters and by subsampling the resulting image by a factor 2^j. The details at different resolutions are regrouped into a pyramid structure called the Laplacian pyramid. Blostein [26] applied a pyramid representation in Laplacian-of-Gaussian scale space to texture segmentation. The term *scale space* denotes a representation of the image response to convolution with Laplacian-of-Gaussian filters over a range of scales. Blostein found all regions that have small gray-level variation relative to a neighborhood of their size, then nested regions are constructed whenever small regions are spatially contained within larger regions. Unser [27] suggested that one should utilize local texture properties by using local linear transforms that have been optimized for maximal texture discrimination. Mallat [28] showed that the difference of information between the approximation of a signal at the resolutions 2^{j+1} and 2^j can be extracted by decomposing this signal on a wavelet orthogonal basis $L^2(R^n)$, the vector space of measurable, square-integrable one-dimensional functions. This decomposition defines an orthogonal multiresolution representation called a wavelet representation. It is computed with a pyramidal algorithm based on convolutions with quadrature mirror filters. All these methods need a lot of computational overhead for preprocessing such that the computational complexity cannot be reduced. In this paper, a simple pyramid-like structure with low computational cost is employed to describe the signal details at different resolutions.

Based upon these concepts, a new texture feature called multiresolution fractal (MF) feature vector is proposed to distinguish the three sets of ultrasonic liver images. Fractal dimensions estimated at different resolutions are gathered to form a feature vector. We will show in Section II that the MF feature vector can discriminate two kinds of texture with the same fractal dimension but different appearances; that is to say, the feature vector contains the information of lacunarity. This feature vector is applied to the classification of the three sets of sample ultrasonic liver images and is compared to the conventional features. From experimental results it can be concluded that our approach is superior to the conventional methods.

This paper is organized as follows. The definitions of the texture features employed in this paper are reviewed (for the conventional features) and proposed (for the new feature-extraction technique) in the next section. The pattern-classification technique utilized and its experimental result are shown in Sections III and IV, respectively. Finally, discussions and conclusions are followed.

II. Features Used

This section describes the classes of features employed in the experiments for the classification of ultrasonic liver images. For each class of features, we find the feature combination that have the best performance as determined by the Hotelling trace criterion described in Section III.

A. The Spatial Gray-Level Dependence Matrices

The spatial gray-level dependence matrices (SGLDM) [9], [11], [29], [30] are based on the estimation of the second-order joint conditional probability density functions, $f(i,j;\, d,\theta)$. Each $f(i,j;\, d,\theta)$ is the probability of going from gray-level i to gray-level j, given that the intersample spacing is d and the direction is specified by the angle θ. The estimated values for these probability density functions will be denoted by $P(i,j;\, d,\theta)$. Formally, for angles quantized to 45° intervals the estimated joint conditional probability density functions are defined by

$$P(i,j;\, d,0^\circ) = \#\{((k,l),(m,n)) \in (L_y \times L_x) \times (L_y \times L_x) : k = m,\ |l-n| = d, I(k,l) = i,\ I(m,n) = j\} / T(d,0^\circ). \tag{2}$$

$$P(i,j;\, d,45^\circ) = \#\{((k,l),(m,n)) \in (L_y \times L_x) \times (L_y \times L_x) : (k-m = d,\ l-n = -d) \text{ or } (k-m = -d,\ l-n = d),\ I(k,l) = i,\ I(m,n) = j\} / T(d,45^\circ), \tag{3}$$

$$P(i,j;\, d,90^\circ) = \#\{((k,l),(m,n)) \in (L_y \times L_x) \times (L_y \times L_x) : |k-m| = d, l = n,\ I(k,l) = i,\ I(m,n) = j\} / T(d,90^\circ) \tag{4}$$

$$P(i,j;\, d,135^\circ) = \#\{((k,l),(m,n)) \in (L_y \times L_x) \times (L_y \times L_x) : (k-m = d,\ l-n = d) \text{ or } (k-m = -d,\ l-n = -d),\ I(k,l) = i,\ I(m,n) = j\} / T(d,135^\circ) \tag{5}$$

where $\#$ denotes the number of elements in the set, L_x and L_y are the horizontal and vertical spatial domains, $I(x,y)$ is the image intensity at point (x,y), and $T(d,\theta)$ stands for the total number of pixel pairs within the image which have the intersample spacing d and direction angle θ. $P(i,j;\, d,\theta)$ measures the probability that the intensities of a pixel pair (k,l) and (m,n), within the image which have the intersample spacing d and direction angle θ or $\theta + 180^\circ$, are i and j, respectively.

Each of the estimated joint probability density functions can be written in matrix form

$$\boldsymbol{M}(d,\theta) = [P(i,j;\, d,\theta)].$$

If texture is coarse, and d is small compared to the sizes of the texture elements, the pairs of points at separation distance d should usually have similar gray level. This means that $P(i,j;\, d,\theta)$ is large for $i \cong j$, i.e., the high values in the matrix $\boldsymbol{M}(d,\theta)$ should be concentrated on or near its main diagonal. Conversely, for fine texture, the gray levels of points separated by distance d should often be quite different, so that $P(i,j;\, d,\theta)$ are almost equal for all i and j; i.e., the values in $\boldsymbol{M}(d,\theta)$ should be spread out relatively uniformly. Thus, a good way to analyze texture coarseness would be to compute, for various values of d, some measure of the scatter of the $\boldsymbol{M}(d,\theta)$ values around the main diagonal.

Haralick [9] proposed 14 measures that can be employed to extract useful texture information from $\boldsymbol{M}(d,\theta)$ matrices. Two of the measures are applied to the detection of diffuse liver diseases since they have the best performance among the 14 features in our experiments (The feature selection scheme will be described in Section IV). They are as follows.

1) *Correlation:*

$$\text{COR} = \sum_i \sum_j [ijP(i,j;\, d,\theta) - \mu_x \mu_y] / (\sigma_x, \sigma_y) \tag{6}$$

where μ_x and σ_x are the mean and standard deviation of the row sums of the matrix $\boldsymbol{M}(d,\theta)$, and μ_y and σ_y are the corresponding statistics of the column sums.

2) *Sum Entropy:*

$$\text{SE} \equiv -\sum_i M_{x+y}(i) \log M_{x+y}(i) \tag{7}$$

where $M_{x+y}(i)$ is defined as

$$M_{x+y}(i) = \sum_{\substack{m \\ m+n=i}} \sum_{\substack{n \\ m+n=i}} P(m,n;\, d,\theta).$$

Each measure is evaluated for $d = 1$ and $\theta = 0^\circ$, 45°, 90°, 135°. The desired features are obtained from the sample mean and standard deviation of the estimated values.

B. The Fourier Power Spectrum

To use the Fourier power spectrum (FPS) [10], [11], [29], [31] one must first compute the sample power spectrum,

$$\phi(u,v) \equiv F(u,v)F^*(u,v) = |F(u,v)|^2$$

where ϕ is the sample power spectrum, * denotes the complex conjugate, and F stands for the Fourier transform of the image. Coarse texture will have high values of $|F|^2$ concentrated near the origin, while in fine texture the values will be more spread out. Similarly, texture with many edges or lines in a given direction θ will have high values of $|F|^2$ concentrated around the perpendicular direction $\theta + \frac{\pi}{2}$, while in homogeneous texture, $|F|^2$ should be nondirectional.

Annular-ring and wedge sampling geometries are commonly used for FPS features, which are defined as follows:

$$\phi_{r_1,r_2} \equiv \sum_{r_1^2 \le u^2+v^2 < r_2^2} |F(u,v)|^2,$$
$$\phi_{\theta_1,\theta_2} \equiv \sum_{\theta_1 \le \tan^{-1}(v/u) \le \theta_2} |F(u,v)|^2 \qquad (8)$$

where $0 < u, v < M-1$ for a given $M \times M$ image.

The ring ϕ_{r_1,r_2} and wedge ϕ_{θ_1,θ_2} applied to the classification of ultrasonic liver images are $\phi_{2,4}$ and $\phi_{0^\circ,45^\circ}$ since better results can be obtained than any other combination of rings and wedges.

C. The Gray-Level Difference Statistics

To describe the gray-level difference statistics (GLD) [11], let $I(x,y)$ be the image intensity function. For any given displacement $\delta \equiv (\Delta x, \Delta y)$, let $I_\delta(x,y) \equiv |I(x,y) - I(x+\Delta x, y+\Delta y)|$, and p_δ be the probability density of $I_\delta(x,y)$. If there are m gray levels, this has the form of an m-dimensional vector whose ith component is the probability that $I_\delta(x,y)$ will have value i. It is easy to compute p_δ by counting the number of times each value of $I_\delta(x,y)$ occurs where Δx and Δy are integers.

If texture is coarse, and δ is small compared to the texture element size, the pairs of points at separation δ should usually have similar gray levels, so that $I_\delta(x,y)$ should usually be small, i.e., the values in p_δ should be concentrated near $i = 0$. Conversely, for fine texture, the values in p_δ should be more spread out. Thus, a good way to analyze texture coarseness would be to compute, for various magnitudes of δ, some measure of the spread of values in p_δ away from the origin. The feature used to classify the three sets of ultrasonic liver images is the entropy which is defined by

$$\mathrm{ENT} \equiv -\sum_i P_\delta(i) \log P_\delta(i) \qquad (9)$$

since they perform the best results in our experiments. The entropies are estimated for $\delta = (3,0)$, $(3,3)$, $(-3,3)$, and (0,3) and take the sample mean and standard deviation.

D. Laws' Texture Energy Measures

Laws' texture energy measures (TEM) [12], [32] are derived from three simple vectors of length 3, $L3 \equiv (1,2,1)$, $E3 \equiv (-1,0,1)$, and $S3 \equiv (-1,2,-1)$, which represent the one-dimensional operations of center-weighted local averaging, symmetric first differencing for edge detection, and second differencing for spot detection. If these vectors are convolved with themselves or with each other, we obtain five vectors of length 5, $L5 \equiv (1,4,6,4,1)$, $S5 \equiv (-1,0,2,0,-1)$, $R5 \equiv (1,-4,6,-4,1)$, $E5 \equiv (-1,-2,0,2,1)$, and $W5 \equiv (-1,2,0,-2,1)$ where $L5$ again performs local averaging, $S5$ and $E5$ are, respectively, spot and edge detectors, and $R5$ and $W5$ can be regarded as "ripple" and "wave" detectors. If we multiply the column vectors of length 5 by row vectors of the same length, we obtain Laws' 5×5 masks. To use these masks to describe texture in an image, we convolve them with the image and use statistics (e.g., energy) of the results as texture properties. The masks used in our experiments are two of the zero-sum masks

$L5^tE5$

−1	−2	0	2	1
−4	−8	0	8	4
−6	−12	0	12	6
−4	−8	0	8	4
−1	−2	0	2	1

$L5^tS5$

−1	0	2	0	−1
−4	0	8	0	−4
−6	0	12	0	−6
−4	0	8	0	−4
−1	0	2	0	−1

since they are the best.

E. The Proposed Method

The information measured by the four conventional features are coarseness, regularity, directionality, and energy. One of the most important information, granularity, is not considered by these feature classes. Hence, to obtain useful information from the ultrasonic liver images, we introduce a feature extraction technique which is based on the concepts of multiple resolution imagery and fractional Brownian motion model.

1) Multiple Resolution Feature Extraction: Textural and contextural features are two of the fundamental pattern elements used in human interpretation of pictorial information. Textural features contain information about the spatial distribution of tonal variations within a band of the visible and/or infrared portion of an electromagnetic spectrum, while contextual features contain information derived from blocks of pictorial data surrounding the area being analyzed. When small image areas from black and white photographs are independently processed by a machine, then texture and tone are most important.

Context, texture, and tone are always present in an image, although at times one property can dominate the other. One way of measuring the three data is to visualize the image at different resolutions. The pyramidal approach is one of the popular ways for multiresolution image analysis. Based upon the concept of pyramidal data analysis, we can define the image at resolution level i as

$$I^{(i)}(x,y) = \Big[I^{(i+1)}(2x,2y) + I^{(i+1)}(2x+1,2y) + I^{(i+1)}(2x,2y+1) + I^{(i+1)} \cdot (2x+1,2y+1)\Big] \Big/ 4,$$
$$0 \le i \le m, \quad 0 \le x,y \le 2^i, \qquad (10)$$

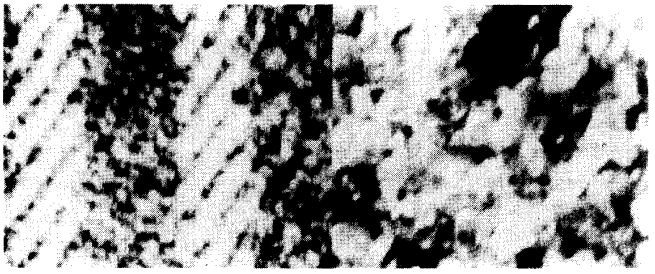

(a) (b)

Fig. 1. Two kinds of image texture with the same fractal dimension but different lacunarities. Their MF feature vector (MF3) are [0.66 0.54 0.20 0.16] and [0.66 0.53 0.36 0.22], respectively.

while $I^{(m)}$ is the original image. The reason for the simplified definition is to lower computational cost.

2) Fractional Brownian Motion Model: The fractional Brownian motion (FBM) model developed by Mandelbrot [16] is used to describe the roughness of nature surfaces. It regards naturally occurring surfaces as the end result of random walks. Such random walks are basic physical processes in our universe. An intensity surface of an ultrasonic image can also be viewed as the end result of a random walk, so the FBM model can be suitable for the analysis of ultrasonic liver images.

One of the most important parameters to represent a fractal surface is the fractal dimension. Theoretically, the fractal dimension D_f is estimated from the equation

$$E(\Delta I^2) = c(\Delta r)^{(6-2D_f)}$$

where $E(\cdot)$ denotes the expectation operator, $\Delta I \equiv I(x_2, y_2) - I(x_1, y_1)$ is the intensity variations, c is some constant, and $\Delta r \equiv \|(x_2, y_2) - (x_1, y_1)\|$ is the spatial distance. A simpler method is to estimate the H parameter from the relationship

$$E(|\Delta I|) = k(\Delta r)^H \tag{11}$$

where $k = E(|\Delta I|)_{\Delta r=1}$. If we apply the log function to both sides of (11), we obtain

$$\log E(|\Delta I|) = \log k + H \log(\Delta r). \tag{12}$$

From (12), we can deduce a procedure to estimate the H parameter and the fractal dimension can be easily computed from the relationship

$$D_f = 3 - H. \tag{13}$$

A small value of fractal dimension D_f (large value of parameter H) means a smooth surface, and large D (small H), a rough surface.

Given an $M \times M$ image I, the intensity difference vector is defined as IDV $\equiv [id(1), id(2), \cdots, id(s)]$ where s is the maximum possible scale and $id(k)$ is the average of the absolute intensity difference of all pixel pairs with horizontal or vertical distance k, and see (14) below. Value of H can be obtained by using least-squares linear regression to estimate the slope of the curve of $id(k)$ versus k in log–log scales.

3) Multiresolution Fractal Feature Vector: Based on the concepts described as above, the multiresolution fractal (MF) feature vector is defined as

$$MF \equiv \left(H^{(m)}, H^{(m-1)}, \cdots, H^{(m-n+1)}\right) \tag{15}$$

where $M = 2^m$ is the size of the original image, $H^{(k)}$ is the H parameter estimated from image $I^{(k)}$, and n is the number of resolution levels chosen in our experiments.

The feature vector describes not only the roughness but also the lacunarity of the image. Consider the two images shown in Fig. 1 which have the same fractal dimension (2.34) but different lacunarities [0.33 and 0.37, measured by means of (1)], the corresponding MF feature vectors are shown on the bottom of the images. The intensity values of these textures were approximated by a fractal Brownian function [i.e., fitting (12)] and the approximation error observed. We have found that the approximation is quite good—implying that the intensity surfaces of the textures are actually a fractal Brownian functions. Thus, the estimation error of the H parameter can be ignored (in our experiences, the error is less than 5%). It can be found that the fractal dimensions at resolution levels $m-2$ and $m-3$ are quite different for the two images. In this way, the separation of textures with the same fractal dimensions can be made by considering all but the first components of their MF feature vectors.

In addition to the roughness and lacunarity information contained in the MF feature vector, some other phenomena can also be described by the feature vector. Consider the

$$id(k) = \frac{\sum_{x=0}^{M-1}\sum_{y=0}^{M-k-1}|I(x,y) - I(x,y+k)| + \sum_{x=0}^{M-k-1}\sum_{y=0}^{M-1}|I(x,y) - I(x+k,y)|}{2M(M-k-1)}. \tag{14}$$

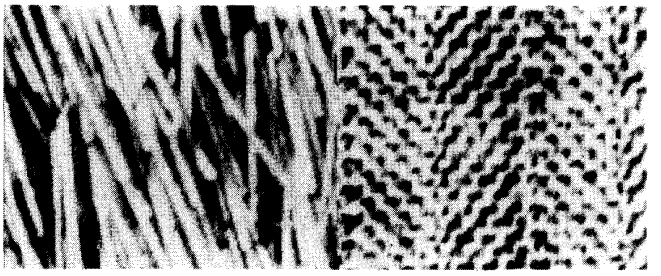

(a) (b)

Fig. 2. Two kinds of image texture with the same fractal dimension and lacunarities. Their MF feature vector (MF3) are [0.67 0.39 0.17 0.00] and [0.67 0.27 –0.22 –0.05], respectively.

images shown in Fig. 2 which have the same fractal dimension (2.33) and lacunarity (0.21) but different appearances. We can discriminate them by the difference between their MF feature vectors. One observable phenomenon to distinguish between these two images is their regularities, Fig. 2(a) is arranged more randomly than Fig. 2(b). This means that the MF feature vector can also describe the regularity of an image.

III. Pattern Classification Technique

The Bayes classifier is applied to probe the feasibility of classifying tissue types as well as determining some properties of various feature spaces. From the statistical point of view, the Bayes classifier represents the optimum measure of performance.

One of the ways to represent a pattern classifier is in terms of a set of *discriminant functions* $g_i(X)$, $i = 1, \cdots, K$ where K is the number of classes. The classifier is said to assign a feature vector X to class w_i if $g_i(X) > g_j(X)$ for all $j \neq i$. Let us assume that the distribution of the feature vectors X within the ith class $P(X|w_i)$ is a multivariate normal (Gaussian) with mean vector $\boldsymbol{\mu_i}$ and covariance matrix C_i. For the Bayes classifier, the discriminant functions can be defined as

$$g_i(X) \equiv \log P(X|w_i) + \log P(w_i)$$

where $P(w_i)$ is the *a priori* probability of class w_i. Assume that the *a priori* probabilities are equal for all classes. Then it is easy to obtain the discriminant functions

$$g_i(X) = -\frac{1}{2}(X - \boldsymbol{\mu_i})^t C_i^{-1}(X - \boldsymbol{\mu_i}) - \frac{1}{2}\log|C_i|. \quad (16)$$

To measure the overall diagnostic performance of the feature vectors, the Hotelling Trace Criterion (HTC) [15] is employed. The HTC is a simple method of evaluating the intrinsic separability of a tissue signature that is faster and easier to calculate. The HTC is expressed by the scalar quantity

$$J = \text{trace}(S_w^{-1} S_b) \quad (17)$$

where S_w and S_b are the within- and between-class scatter matrices defined by

$$S_w = \sum_{i=1}^{K} P(w_i) C_i,$$

$$S_b = \sum_{i=1}^{K} P(w_i)\left(\boldsymbol{X}^{(i)} - \boldsymbol{X}^{(0)}\right)\left(\boldsymbol{X}^{(i)} - \boldsymbol{X}^{(0)}\right)^T,$$

where $\boldsymbol{X}^{(i)}$ is the expected vector of the ith class and $\boldsymbol{X}^{(0)} = \sum_{i=1}^{K} P(w_i)\boldsymbol{X}^{(i)}$ is the expected vector of the mixture. The HTC is useful in selecting the best feature combination for classification. Therefore, features with maximum J may be selected.

To compare the performance of the features described previously, we define the correct classification rate as

$$\text{CR} \equiv \sum_{i=1}^{K} P(w_i)\frac{n_i}{N_i} \quad (18)$$

where n_i is the number of correctly classified samples out of a total of N_i from the ith class.

IV. Experimental Results

A. Data Acquisition and Feature Selection

In this paper, all ultrasonic images are captured from a phased-array system (Aloka SSD-265, Tokyo, Japan) with a 3.5 MHz (dynamic focusing) transducer. The images are transferred through the Itex-100 vision interface board to a PC-AT personal computer and are digitized with 512 × 512 pixel and 256 gray-level resolution. The size of the tissue is indicated by the ruler on the top of Fig. 3(a). The resultant images are then transmitted through the NFS network system to a SUN 4/330 workstation for further processing. Three sets of ultrasonic liver images, each of 30 samples from 15 patients (2 samples per patient), are taken by the same physician and on the same ultrasonic scanner. Fig. 3(a) shows one of the normal liver images, while Fig. 3(b) and (c) show the hepatoma and cirrhosis cases, respectively. For each sampled image, a block of 32 × 32 pixels (shown in Fig. 3 with white rectangle) is selected as the data to be analyzed in the sequel. The block is chosen, if possible, to include solely liver parenchyma without major blood vessels.

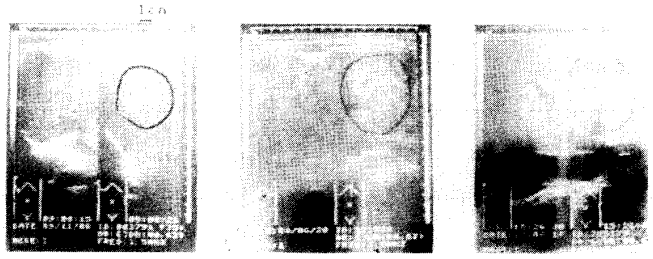

(a) (b) (c)

Fig. 3. Sampled ultrasonic liver images. The image in (a) is the normal liver. The images in (b) and (c) are hepatoma and cirrhosis, respectively.

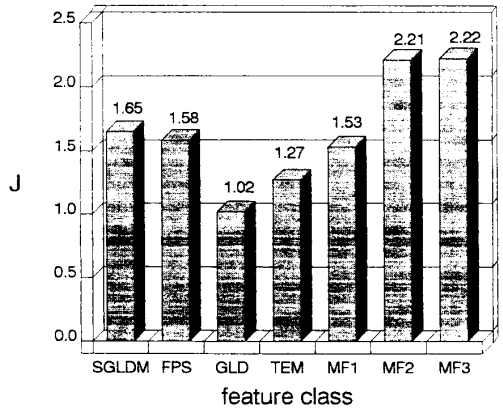

Fig. 4. Measures of the performance of the features used to classify the three sets of ultrasonic liver images. The feature classes are summarized in Table I.

TABLE I
FEATURE SETS USED FOR THE CLASSIFICATION OF ULTRASONIC LIVER IMAGES

Feature Class	Features Used	Feature Length
SGLDM	Correlation (COR) and Sum Entropy (SE)	4
FPS	Ring [2, 4) and Wedge [0, 45]	2
GLD	Entropy (ENT)	2
TEM	L5E5 and L5S5	2
MF1	MF with resolution levels 5 and 4	2
MF2	MF with resolution levels 5, 4, and 3	3
MF3	MF with resolution levels 5, 4, 3, and 2	4

TABLE II
CLASSIFICATION PERFORMANCE OF THE FEATURES USED IN THIS PAPER

Feature Class	CR
SGLDM	83.3%
FPS	80.0%
GLD	74.4%
TEM	71.1%
MF1	80.0%
MF2	88.9%
MF3	87.8%

For each class of the four conventional texture features described in Section II, the combined features that perform the best result will be selected as the feature vector in our experiments. The selection scheme is based on the concept of HTC. For example, let us consider the 14 features associated with the spatial gray level dependence matrices, values of J are calculated for any combination of the features. The combined features with maximum J are used to classify the three sets of ultrasonic liver images. The selected features for each feature class are described in Section II and summarized in Table I. Values of J for the selected features are plotted in Fig. 4.

For the proposed method, n various resolution images denoted as $I^{(m)}$, $I^{(m-1)}$, $\cdots$, $I^{(m-n+1)}$ where $m = \log_2 M = 5$, are obtained from each sample block by means of (10). The corresponding fractal dimensions of these images are computed from (12) and (13) and are gathered to form the MF feature vector as (15). The maximum possible scale used to estimate the fractal dimension is $s = 3$. For example, consider the image $I^{(k)}$, the components of its intensity difference vector, $\mathrm{id}(k) = 1, 2, 3$, are computed by using (14). Slope of the curve of $\mathrm{id}(k)$ versus k in log–log scales is estimated by using a least-squares linear regression scheme. From the estimated slope, the fractal dimension can be easily computed from (13). The estimated MF feature vectors with various resolution levels (MF1, MF2, and MF3 shown in Table I) are used to classify the three types of ultrasonic liver images. Values of J for these feature vectors are also shown in Fig. 4.

B. Classification Results

The 90 sampled ultrasonic liver images are classified into the three classes (i.e., normal, hepatoma, and cirrhosis), using the selected feature vectors and the pattern classification techniques described in Sections II and III. All programs are written in C language and executed on a SUN 4/330 workstation. The execution time and the correct classification rates by using these features are shown in Fig. 5 and Table II, respectively.

We first analyze the classification errors of the four conventional features. Their confusion matrices are listed out in Table III. From the experimental results we have found that the feature vector selected from the SGLDM feature class has the best performance among the four feature classes, which is consistent with the results obtained by Weszka [11] for terrains classification. This is reasonable since a theoretical comparison of the features [33] affirmed that the SGLDM is better than the others. Contrary to the SGLDM, Laws'

TABLE III
CONFUSION MATRICES FOR THE TEXTURE FEATURES USED IN THIS PAPER. N = NORMAL LIVER, H = HEPATOMA, AND C = CIRRHOSIS

correct class	classified as N	H	C
N	25	1	4
H	4	26	0
C	3	3	24

(a) SGLDM

correct class	classified as N	H	C
N	26	0	4
H	0	27	3
C	10	1	19

(b) FPS

correct class	classified as N	H	C
N	24	1	5
H	2	27	1
C	7	7	16

(c) GLD

correct class	classified as N	H	C
N	23	1	6
H	4	23	3
C	6	6	18

(d) TEM

correct class	classified as N	H	C
N	23	2	5
H	6	23	1
C	1	3	26

(e) MF1

correct class	classified as N	H	C
N	26	1	3
H	2	28	0
C	2	2	26

(f) MF2

correct class	classified as N	H	C
N	25	1	4
H	2	28	0
C	3	1	26

(g) MF3

TEM feature that measures the edginess of an image has the worst performance. We are not surprised with this result since the quality of an ultrasonic image is so poor that the edges are almost produced by noises. This problem may be solved by preprocessing (smoothing) or using the technique of nonmaximum suppression [32]; but, anyway, this method is not favorable because of its time consumption and low accuracy.

By inspection of the confusion matrices, we have found that the FPS feature is perfect for the discrimination of normal livers and hepatoma, i.e., their is no misclassification samples between these two sets of ultrasonic liver images. This is an encouraging result which suggests to us to select FPS as feature to detect abnormal livers. If a sample is recognized to be hepatoma, then we can be absolutely sure that the sample is abnormal (may be hepatoma or cirrhosis.)

Another phenomenon, which functions as complementary interaction, can be observed by further investigation of the classification errors. Some sample images are misclassified by one of the feature classes but correctly classified by another. For example, samples 23, 25, and 28 of normal data set are misclassified by using the SGLDM feature but can be classified by using the FPS feature. Similarly, samples 2 and 21 of the same data set are misclassified by using the FPS feature but correctly classified by the SGLDM feature. Hence, it is expected that the combination of these two feature classes will have a better performance. The classification results and their confusion matrices of any combination of the four feature classes are shown in Tables IV and V, respectively. Three observations can be obtained from the tables.

TABLE IV
ANY COMBINATION OF THE FOUR CONVENTIONAL FEATURE CLASSES AND THEIR PERFORMANCE

Combined Features	Feature Length	J	CR
SGLDM & FPS	6	3.06	84.4%
SGLDM & GLD	6	1.79	84.4%
SGLDM & TEM	6	2.02	74.4%
FPS & GLD	4	2.70	80.0%
FPS & TEM	4	2.79	82.2%
GLD & TEM	4	1.36	77.8%

i) As was expected, the combination of SGLDM and FPS has a little improvement of the SGLDM. The performance of the combined feature is almost the same as that of the physical properties based features [4]. This is reasonable since both feature sets are based on the evaluation of the autocorrelation or power spectrum of the image.

ii) Although, the ability of distinguishing between abnormalities are enhanced, one of the drawbacks of the combined feature, see Table V(b), is that the number of misclassified normal sample is increased, which means that the probability of recognizing a normal liver as abnormal is increased. Hence, for prac-

TABLE V
CONFUSION MATRICES FOR THE COMBINED TEXTURE FEATURES. N = NORMAL LIVER, H = HEPATOMA, AND C = CIRRHOSIS

correct class	classified as N	H	C
N	23	1	6
H	1	29	0
C	5	1	24

(a) SGLDM and FPS

correct class	classified as N	H	C
N	25	1	4
H	1	28	1
C	4	3	23

(b) SGLDM and GLD

correct class	classified as N	H	C
N	23	2	5
H	6	24	0
C	8	2	20

(c) SGLDM and TEM

correct class	classified as N	H	C
N	24	0	6
H	2	28	0
C	9	1	20

(d) FPS and GLD

correct class	classified as N	H	C
N	24	0	6
H	0	28	2
C	7	1	22

(e) FPS and TEM

correct class	classified as N	H	C
N	24	1	5
H	2	24	4
C	6	2	22

(f) GLD and TEM

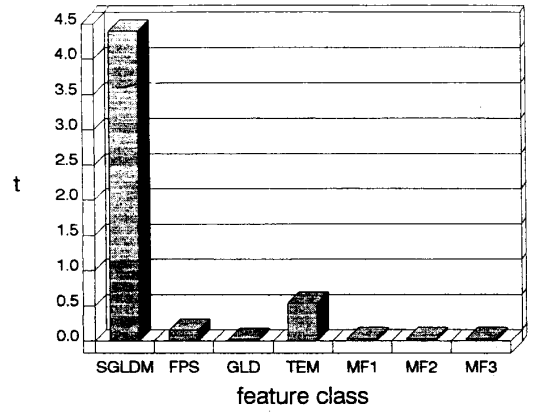

Fig. 5. Execution time of the features used in this paper: time is given in seconds and referred to CPU time of a SUN 4/330 workstation.

Feature Class	Time
1. SGLDM	4.4
2. FPS	0.16
3. GLD	0.023
4. TEM	0.54
5. MF1	0.034
6. MF2	0.035
7. MF3	0.036

tical consideration, SGLDM is the best useful texture feature.

iii) Intuitively, one might expect that the performance to be improved, or at least unchanged, by making additional measurements on the images. However, Devijver [8] has pointed out that the overall detectability may decrease by including a correlated feature with marginal or no discriminability. In other words, since every element of a feature has its contribution to the classification performance, it will be degraded when the added feature elements have bad geometrical distribution, i.e., the distribution spreads over the feature space. This behavior can be found in Table V(c) where the performance of SGLDM is degraded to 74% for the bad geometrical distribution of the feature elements of TEM.

Besides of accuracy, speed is another important consideration in practical application. For the consideration of accuracy, SGLDM is the best; as to the speed, SGLDM is the worst. Since the size of spatial gray-level dependence matrix is dependent on the resolution levels of the image, one way to reduce the computation complexity of SGLDM should be using a smaller number of gray levels to code the digitized image. For example, we can requantize the original image into 64 resolution levels, which preserves the accuracy and save about 4 times of floating operations. However, this is not fast enough, either. For real time consideration, GLD may be a perfect choice if we ignore its drawback of low accuracy.

To analyze the classification results of the proposed features, their confusion matrices are shown in Table III. In comparison with other methods, we have found that our method with three resolution levels (MF2) has the best performance. This is reasonable since, as stated previously, the MF feature vector contains the information of roughness and lacunarity (or granularity) which are two of the most important properties in describing the ultrasonic liver images. Generally speaking, the more resolution levels are used in our approach the more information is described by the feature vector, and the more accuracy could be obtained. In other words, MF3 (with 4 resolution levels) would have less classification error than MF2. Unfortunately, this is not true since the accuracy of the estimated H parameter is influenced by the size of the image. In our experiments, the size of the image $I^{(2)}$ is only 4×4; i.e., only 16 pixel intensities can be used to estimate the parameter $H^{(2)}$, which will cause a lot of estimation errors. To overcome this problem, a larger block could be chosen to classify the three types of liver tissues more accurately. But,

TABLE VI
COMBINATION OF MF2 AND ANY CONVENTIONAL FEATURE CLASS AND THEIR PERFORMANCE

Combined Features	Feature Length	J	CR
MF2 & SGLDM	7	2.85	88.9%
MF2 & FPS	5	3.24	90.0%
MF2 & GLD	5	2.76	84.4%
MF2 & TEM	5	2.83	82.2%

TABLE VII
CONFUSION MATRICES FOR THE COMBINED TEXTURE FEATURES OF MF2 AND ANY CONVENTIONAL FEATURE CLASS. N = NORMAL LIVER, H = HEPATOMA, AND C = CIRRHOSIS

	classified as		
correct class	N	H	C
N	26	0	4
H	1	29	0
C	4	1	25

(a) MF2 and SGLDM

	classified as		
correct class	N	H	C
N	26	0	4
H	0	30	0
C	3	2	25

(b) MF2 and FPS

	classified as		
correct class	N	H	C
N	26	1	3
H	3	27	0
C	6	1	23

(c) MF2 and GLD

	classified as		
correct class	N	H	C
N	26	1	3
H	2	27	1
C	8	1	21

(d) MF2 and TEM

in general, this is unrealistic since given the resolution of state of the art medical ultrasound images, the block free of major vessels or other gross structures in the liver will be small.

By further inspection of the classification results, again, the complementary interaction phenomenon can be observed. Hence, we combine the MF2 feature vector with any conventional feature class and evaluate their performance. The classification results and their confusion matrices are shown in Tables VI and VII respectively. From the tables we have found that the performance of MF2 is improved by using the combination of MF2 and FPS. The major improvement of the combined feature is that in the hepatoma data set, which combine the advantages of FPS (no misclassification between normal liver and hepatoma) and MF2 (samples of hepatoma is never classified as cirrhosis). However, the major disadvantages of the combined feature is two-fold: 1) the probability of misclassifying a cirrhosis sample is increased and 2) it consumes more time than that of MF2 such that a real time implementation is impossible. Hence, we suggest that the MF2 is good enough for the classification of liver tissues.

V. DISCUSSION AND CONCLUSION

Ultrasound B-scan images have the various granular structure described by texture. In general, texture can be evaluated as being fine, coarse, or smooth; rippled, moiled, irregular, or lineated. In this paper, we have applied four conventional texture features to the description of these phenomena and tried to find the most useful information for the classification of ultrasonic liver images. From the results reported in Section IV, the correlation feature extracted from the SGLDM has the best performance. In fact, the correlation feature is a measure of gray-tone linear-dependencies in the image. From the 90 sampled ultrasonic liver images, we have observed that a normal liver would have a fine structure; in other words, a normal liver image consists mostly of sampled signals which are less correlated to their neighbors such that the correlation feature of a normal liver image has lower value compared to an abnormal one.

Low computational complexity and high accuracy are two of the most important considerations for the classification of ultrasonic liver images. The accuracy of the SGLDM may be acceptable; but the time needed to compute the correlation feature is intolerable. In our experiments, since all images are digitized with 256 gray-level resolution, the size of the spatial gray-level dependence matrix is 256×256. All elements of the matrix should be used to estimate the correlation feature, i.e., $256^2 \left(= 2 \times 32^3\right)$ logarithmic operations are needed to compute the feature. To overcome the problem of time consumption induced by the SGLDM method, we consider the GLD method which uses only a 256-dimensional vector instead of the 256×256 matrix to describe texture surfaces. Thus, the computational cost is dominated by the calculation of the vector, i.e., only 32^2 subtractions are used to obtain the 256-dimensional vector. The major disadvantage of the GLD method is that there is no simple analogy of the correlation measure of SGLDM such that it is less accurate in the classification of ultrasonic liver images.

In this paper, we have proposed a new texture feature based on the concepts of multiple resolution imagery and fractional Brownian motion model. The use of multiresolution is to describe the relationships among contextual, texture, and tone information of the image; while fractal model is employed to measure the degrees of roughness (granularity) of the image

surface. Recently, Chen [21] has suggested that the fractal features can be applied to detect diffuse liver diseases. He used the normalized fractional Brownian motion (NFBM) feature vector to discriminate five normal and abnormal ultrasonic liver images. Again, time consumption is also the major disadvantage of NFBM feature vector. All pixel pairs within the image should be considered to computer the NFBM feature vector. Consider a 32×32 image, 32^4 operations are needed to extract the NFBM features from the image. In our approach, we only consider the horizontal and vertical pixel pairs (pixel pairs whose elements are located on the same row or column), this will save a lot of computations.

To evaluate the performance of these features, the Bayes classifier and the Hotelling trace criterion are utilized. The performance of a classifier is strongly affected by the ratio of the training size per class, N ($= 15$ in our experiments), to the dimensionality of the feature space, L. In general, it is better to have a larger N/L to avoid bias in the estimation of the J values and the classification rates (CR). The J values in our experiments are larger than 1, which is never found in the experiments of Insana [6]. This may be due to the following facts: 1) the bias caused by the lower N/L ratio and 2) there are three classes (only two classes in [6]) of liver samples should be classified. Although it is recognized that the greater ratio of N/L the better the results, Foley [34] pointed out that a reasonable engineering rule of thumb that if the ratio of sample to feature size is greater than three, then on the average the training-set error rate is reasonably close to the test-set error rate. In our experiments, most feature vectors satisfy this condition ($L < 5$).

From experimental results, we have found that the performance of the MF feature vector is influenced by the number of resolution levels used and the size of the original image. The size of the image will determine the variation of the estimated H parameter. The smaller the image size is, the larger the estimated error of the H parameter will be. This phenomenon can be proved by the experimental results that the classification error caused by MF3 (with 4 resolution levels) is larger than that of MF2 (with 3 resolution levels). In general, the MF features with more resolution levels should have a better performance since more information is contained in the features. In our experiments, the size of the image $I^{(2)}$ is so small that the estimated H parameter is unacceptable. This is the reason why MF3 performs no better than MF2. In practice, the size of the image used to estimate the H parameter is at least 8×8.

The physiological factors of the three kinds of liver tissue that cause differences in the MF2 can be interpreted as follows. The most common and characteristic form of the hepatocellular carcinoma (hepatoma) is the trabecular pattern. Tumor cells are arranged in anastomosing plates separated by a sinusoidal network. The structure thus resembles that of normal liver, but the trabeculate are usually wider and less regular [35]. Hence, at a glance of the hepatoma liver image, it is rougher than a normal liver image and has a larger lacunarity. Consequently, $H^{(5)}$ and $H^{(4)}$ of a hepatoma liver image are larger than that of a normal liver image, but $H^{(3)}$ is smaller than that of a normal liver image since the lacunarity of the former is larger than that of the latter. The major characteristic of liver cirrhosis is the hepatic fibrosis associated with beginning nodules or fully established nodules [36]. The nodules cause a block structure in the image such that $H^{(5)}$ of a cirrhosis liver image is larger than that of a normal liver image but smaller than that of a hepatoma liver image.

The reasons for the classification errors of MF feature vector are summarized as follows.

i) It is well known that the estimated fractal dimension is sensitive to noise. Since the quality of ultrasound image is not good enough such that a lot of noises may be imposed on the image, which will cause some estimation errors of the fractal dimensions.

ii) Some blood vessels may be included in the images. Although we are careful in selecting the image block, small blood vessels which destroy the homogeneous structure of the image may still be included in the block.

iii) In addition to roughness and granularity, some other important information should also be considered. For example, the combination of MF2 and FPS has a little improvement of MF2; that is to say, regularity and directionality described by FPS are also important features for the classification of ultrasonic liver images.

iv) As the reasons stated at the start of Section I, some important information may be lost by using a B-scan image.

However, the experimental results show that the MF feature vector is computationally fast and accurate in classifying the three types of ultrasonic liver images. This suggests that the MF feature vector is an excellent tool in analyzing the ultrasonic liver images. Further applications of the MF feature vector are being studied.

REFERENCES

[1] M. F. Insana, R. F. Wagner, B. S. Garra, D. G. Brown, and T. H. Shawker, "Analysis of ultrasound image texture via generalized Rician statistics," *Opt. Eng.*, vol. 25, pp. 743–748, 1986.

[2] U. Reath, D. Schlaps, and B. Limberg, "Diagnostic accuracy of computerized B-scan texture analysis and conventional ultrasonography in diffuse parenchymal and malignant liver disease," *J. Clin. Ultrasound*, vol. 13, pp. 87–99, 1985.

[3] N. M. Botros, "A microprocessor-based pattern recognition algorithm for *in-vivo* tissue differentiation," *J. Clin Eng.*, vol. 13, pp. 115–120, 1988.

[4] R. Momenan, M. H. Loew, M. F. Insana, R. F. Wagner, and B. S. Garra, "Application of pattern recognition techniques in ultrasound tissue characterization," *10th Int. Conf. Pattern Recognition*, vol. 1, pp. 608–612, 1990.

[5] M. F. Insana, R. F. Wagner, B. S. Garra, R. Momenan, and T. H. Shawker, "Pattern recognition methods for optimizing multivariate tissue signatures in diagnostic ultrasound," *Ultrason. Imaging*, vol. 8, pp. 165–180, 1986.

[6] B. S. Garra, M. F. Insana, T. H. Shawker, R. F. Wagner, M. Bradford, and M. Russell, "Quantitative ultrasonic detection and classification of diffuse liver disease comparison with human observer performance," *Invest. Radiol.*, vol. 24, pp. 196–203, 1989.

[7] R. F. Wagner, M. F. Insana, and G. Brown, "Unified approach to the detection and classification of speckle texture in diagnostic ultrasound," *Opt. Eng.*, vol. 25, no. 6, pp. 738–742, 1986.

[8] F. L. Lizzi, M. Ostromogilsky, E. J. Feleppa, M. C. Rorke, and M. M. Yaremko, "Relationship of ultrasonic spectral parameters to features of tissue microstructure," *IEEE Trans. Ultra. Ferro. Freq. Control*, vol. UFFC-34, pp. 319–329, 1986.

[9] R. M. Haralick, K. Shanmugan, and I. H. Dinstein, "Texture features for image classification," *IEEE Trans. Syst., Man, Cyber.*, vol. SMC-3, pp. 610–621, 1973.

[10] G.O. Lendaris and G.L. Stanley, "Diffraction pattern sampling for automatic pattern recognition," *Proc. IEEE,* vol. 58, pp. 198–216, 1970.
[11] J.S. Weszka, C.R. Dryer, and A. Rosenfeld, "A comparative study of texture measures for terrain classification," *IEEE Trans. Syst., Man, Cybern.,* vol. SMC-6, pp. 269–285, 1976.
[12] K.I. Laws, "Texture energy measures," in *Proc. Image Understanding Workshop,* pp. 47–51, 1979.
[13] R.O. Duda and P.E. Hart, *Pattern Classification and Scene Analysis.* New York: Wiley, 1973, pp. 17–20.
[14] J.T. Tou, and R.C. Gonzalez, *Pattern Recognition Principles.* Reading, MA: Addison–Wesley, 1974, pp. 94–97.
[15] Z.H. Gu and S.H. Lee, "Optical implementation of the Hotelling trace criterion for image classification," *Opt. Eng.,* vol. 23, pp. 727–731, 1984.
[16] B.B. Mandelbrot, *The Fractal Geometry of Nature,* San Francisco, CA: Freeman, 1982.
[17] A. Fournier, D. Fussell, and L. Carpenter, "Computer rendering of stochastic models," *ACM Commun.,* vol. 25, pp. 371–384, 1982.
[18] S. Peleg, J. Naor, R. Hartley, and D. Avnir, "Multiple resolution analysis and classification," *IEEE Trans. Pattern Anal. Machine Intell.,* vol. PAMI-6, pp. 518–523, 1984.
[19] A. Pentland, "Fractal-based description of nature scenes," *IEEE Trans. Pattern Anal. Machine Intell.,* vol. PAMI-6, pp. 667–674, 1984.
[20] T. Lundahl, W.J. Ohley, S.M. Kay, and R. Siffert, "Fractional Brownian motion: A maximum likelihood estimator and its application to image texture," *IEEE Trans. Med. Imaging,* vol. MI-5, pp. 152–161, 1986.
[21] C.C. Chen, J.S. Daponte, and M.D. Fox, "Fractal feature analysis and classification in medical imaging," *IEEE Trans. Med. Imaging,* vol. 8, pp. 133–142, 1989.
[22] R. Voss, "Random fractals: Characterization and measurement," in *Scaling Phenomena in Disordered Systems.* New York: Plenum, 1986.
[23] J.M. Keller, S. Chen, and R.M. Crownover, "Texture description and segmentation through fractal geometry," *Comput. Vision, Graph., Image Processing,* vol. 45, pp. 150–166, 1989.
[24] P.J. Burt and E.H. Adelson, "The Laplacian pyramid as a compact image code," *IEEE Trans. Commun.,* vol. COM-31, pp. 532–540, 1983.
[25] J. Crowley, "A representation for visual information," Robotic Inst. Carnegie–Mellon Univ., Tech. Rep. CMU-RI-TR-82-7, 1987.
[26] D. Blostein and A. Narendra, "Multiscale region detector," *Comput. Vision, Graph. Image Processing,* vol. 45, pp. 22–41, 1989.
[27] M. Unser and M. Eden, "Multiresolution feature extraction and selection for texture segmentation," *IEEE Trans. Pattern Anal. Machine Intell.,* vol. PAMI-11, pp. 717–728, 1989.
[28] S.G. Mallat, "A theory for multiresolution signal decomposition: The wavelet representation," *IEEE Trans. Pattern Anal. Machine Intell.,* vol. PAMI-11, pp. 674–693, 1989.
[29] R.P. Kruger and W.B. Thompson, "Computer diagnosis of pneumoconiosis," *IEEE Trans. Syst., Man, Cybern.,* vol. SMC-4, pp. 40–49, 1974.
[30] E.M. Darling and R.D. Joseph, "Pattern recognition from satellite altitudes," *IEEE Trans. Syst., Sci., Cybern.,* vol. SSC-4, pp. 38–47, 1968.
[31] C.R. Dyer and A. Rosenfeld, "Fourier texture features: Suppression of aperture effects," *IEEE Trans. Syst., Man Cybern.,* vol. SMC-6, pp. 703–705, 1976.
[32] M. Pietikainen, A. Rosenfeld, and L.S. Davis, "Experiments with texture classificaton using averages of local pattern matches," *IEEE Trans. Syst., Man, Cyber.,* vol. SMC-13, pp. 412–426, 1983.
[33] R.W. Conners and C.A. Harlow, "A theoretical comparison of texture algorithms," *IEEE Trans. Pattern Anal. Machine Intell.,* vol. PAMI-2, pp. 204–222, 1980.
[34] D.H. Foley, "Considerations of sample and feature size," *IEEE Trans. Inform. Theory,* vol. IT-18, pp. 618–626, 1972.
[35] P.J. Scheuer, "Pathologic types of hepatic tumors," in *Liver Cell Carcinoma,* P. Bannasch, D. Keppler, and G. Weber, Eds. New York: Kluwer-Academic, 1989, p. 18.
[36] J.H. Lefkowitch, "Pathologic diagnosis of liver disease," in *Hepatology,* D. Zakim and T.D. Boyer, W.B. Sannders, Eds. London, England, p. 719, 1990.